Supporting Information: Stabilized skyrmion phase detected in MnSi nanowires by dynamic cantilever magnetometry

A. Mehlin,[1] F. Xue,[1,2,a)] D. Liang,[3] H. F. Du,[2] M. J. Stolt,[3] S. Jin,[3,b)] M. L. Tian,[2] and M. Poggio[1,c)]

[1)] *Department of Physics, University of Basel, Klingelbergstrasse 82, 4056 Basel, Switzerland*

[2)] *High Magnetic Field Laboratory, Chinese Academy of Science, Shushanhu Road 350, Hefei 230031, Anhui, P. R. China*

[3)] *Department of Chemistry, University of Wisconsin-Madison, 1101 University Avenue, Wisconsin 53706, USA*

(Dated: June 19, 2015)

[a)]Electronic mail: xuef@hmfl.ac.cn

[b)]Electronic mail: jin@chem.wisc.edu

[c)]Electronic mail: martino.poggio@unibas.ch

I. DERIVATION OF CANTILEVER FREQUENCY SHIFT

The energy of our NW-on-cantilever system can be described by the sum of a mechanical energy term, related to the cantilever (approximated here as a simple harmonic oscillator), and a magnetic energy term, related to the attached NW:

$$E = \frac{1}{2}k_0(l_e \sin\theta)^2 + E_m, \tag{S1}$$

where k_0 is the spring constant, l_e is the effective length of the cantilever, θ is the angle of the cantilever free-end with respect to the applied field $\mathbf{H}$, and E_m is the magnetic energy. Given that the Si cantilever and the epoxy used to attach the sample have no magnetic response, the magnetic energy depends uniquely on the properties of the attached NW. The torque acting on the cantilever is given by:

$$\tau = -\frac{\partial E}{\partial \theta} = -k_0 l_e^2 \sin\theta\cos\theta - \frac{\partial E_m}{\partial \theta}. \tag{S2}$$

Since $\theta << 1$ during the measurement, we can expand E_m as a function of θ around $\theta = 0$:

$$E_m(\theta) = E_m|_{\theta=0} + \left(\frac{\partial E_m}{\partial \theta}\bigg|_{\theta=0}\right)\theta + \frac{1}{2}\left(\frac{\partial^2 E_m}{\partial \theta^2}\bigg|_{\theta=0}\right)\theta^2 + ... \tag{S3}$$

Therefore, writing an expression for τ and keeping only terms up to first order in θ, we have:

$$\tau = -k_0 l_e^2\theta - \left(\frac{\partial E_m}{\partial \theta}\bigg|_{\theta=0}\right) - \left(\frac{\partial^2 E_m}{\partial \theta^2}\bigg|_{\theta=0}\right)\theta, \tag{S4}$$

$$\tau = -\left(\frac{\partial E_m}{\partial \theta}\bigg|_{\theta=0}\right) - \left[k_0 l_e^2 + \left(\frac{\partial^2 E_m}{\partial \theta^2}\bigg|_{\theta=0}\right)\right]\theta. \tag{S5}$$

The first term in (S5) produces a constant deflection of the cantilever, while the term proportional to θ determines the cantilever's spring constant. Approximating the cantilever as a simple harmonic oscillator, we have:

$$m_e\ddot{x} + \Gamma\dot{x} = \frac{\tau}{l_e}, \tag{S6}$$

where m_e is the effective mass of the cantilever, Γ is the cantilever's dissipation, and the position of the cantilever free-end $x = l_e \sin\theta$. For $\theta << 1$, $x = l_e\theta$. Therefore,

$$m_e\ddot{x} + \Gamma\dot{x} + \left[k_0 + \frac{1}{l_e^2}\left(\frac{\partial^2 E_m}{\partial \theta^2}\bigg|_{\theta=0}\right)\right]x = -\frac{1}{l_e}\left(\frac{\partial E_m}{\partial \theta}\bigg|_{\theta=0}\right). \tag{S7}$$

Solving this equation of motion we find the angular resonance frequency of the cantilever:

$$\omega = \sqrt{\frac{k_0}{m_e} + \frac{1}{m_e l_e^2}\left(\frac{\partial^2 E_m}{\partial \theta^2}\bigg|_{\theta=0}\right) - \frac{\Gamma^2}{4m_e^2}}. \tag{S8}$$

We define $\omega_0 = \sqrt{\frac{k_0}{m_e}}$ and solve for the angular frequency shift $\Delta\omega = \omega - \omega_0$:

$$\Delta\omega = \omega_0\left(\sqrt{1 + \frac{1}{m_e\omega_0^2 l_e^2}\left(\frac{\partial^2 E_m}{\partial\theta^2}\bigg|_{\theta=0}\right) - \frac{\Gamma^2}{4m_e^2\omega_0^2}} - 1\right). \tag{S9}$$

Since the last two terms in the square-root are small compared to 1, we expand (S9) to first order in these small parameters:

$$\Delta\omega = \frac{\omega_0}{2k_o}\left[\frac{1}{l_e^2}\left(\frac{\partial^2 E_m}{\partial\theta^2}\bigg|_{\theta=0}\right) - \frac{\Gamma^2}{4m_e}\right]. \tag{S10}$$

In practice, the cantilevers used in these experiments show a small enough dissipation that the last term in eq: (S10) is negligible, resulting in:

$$\Delta\omega = \frac{\omega_0}{2k_o l_e^2}\left(\frac{\partial^2 E_m}{\partial\theta^2}\bigg|_{\theta=0}\right). \tag{S11}$$

Since $f_0 = \frac{\omega_0}{2\pi}$ and $\Delta f = \frac{\Delta\omega}{2\pi}$,

$$\Delta f = \frac{f_0}{2k_o l_e^2}\left(\frac{\partial^2 E_m}{\partial\theta^2}\bigg|_{\theta=0}\right). \tag{S12}$$

II. INFERRING MAGNETIZATION FROM FREQUENCY SHIFT FOR M‖H

We now consider a specific case of our NW-on-cantilever experiment in which **H** is parallel to the long-axis of the NW. Since our measurements respond to the samples's average magnetization **M**, we can – for the moment – ignore the spatial modulation of the magnetization within the sample and write an effective magnetic energy as if the NW were a single-domain particle. This treatment allows us to infer the behavior of the average magnetization as a function of the measured frequency shift Δf. Given the NW's high aspect ratio, this effective energy is dominated by a uniaxial shape-induced anisotropy. The magnetic energy of the system can then be expressed as,

$$E_m = -\mu_0\mathbf{H}\cdot\mathbf{M}V + \frac{\mu_0 V}{2}\left[(\mathbf{M}\cdot\hat{n})^2 D_\parallel + (\mathbf{M}\times\hat{n})^2 D_\perp\right], \tag{S13}$$

where μ_0 is the permeability of free space, $\hat{n}$ is the unit vector along the cantilevers long axis (in this experiment $\hat{n}\|\mathbf{H}$), and $D_\parallel$ ($D_\perp$) is the demagnetization factor along (perpendicular to) $\hat{n}$. Since the long-axis of the NW is aligned along $\hat{n}$, we have $D_\perp > D_\parallel$. Given these circumstances and a magnetization **M** whose characteristic dynamics occur on time-scales

much faster than $\frac{1}{f_0} = 500\mu s$, **H** will set the polarization axis for the average magnetization **M**, and $|\mathbf{M}|$ will tend to increase with increasing $|\mathbf{H}|$. Therefore, rewriting (S13) in terms of θ with $\mathbf{M}\|\mathbf{H}$, we have:

$$E_m = -\mu_0 HMV + \frac{\mu_0 M^2 V}{2}\left[D_\parallel \cos^2\theta + D_\perp \sin^2\theta\right]. \tag{S14}$$

Taking the second derivative of this equation with respect to θ we find:

$$\frac{\partial^2 E_m}{\partial\theta^2} = \mu_0 M^2 V(D_\perp - D_\parallel)[\cos^2\theta - \sin^2\theta]. \tag{S15}$$

giving,

$$\left.\frac{\partial^2 E_m}{\partial\theta^2}\right|_{\theta=0} = \mu_0 M^2 V(D_\perp - D_\parallel). \tag{S16}$$

Applying (S12), we can then write,

$$\Delta f = \frac{\mu_0 M^2 V f_0}{2k_0 l_e^2}(D_\perp - D_\parallel). \tag{S17}$$

Solving for M in terms of Δf, we arrive at:

$$M = l_e\sqrt{\frac{2\Delta f k_0}{f_0\mu_0 V(D_\perp - D_\parallel)}}. \tag{S18}$$

III. PROPERTIES OF CANTILEVERS AND NWS

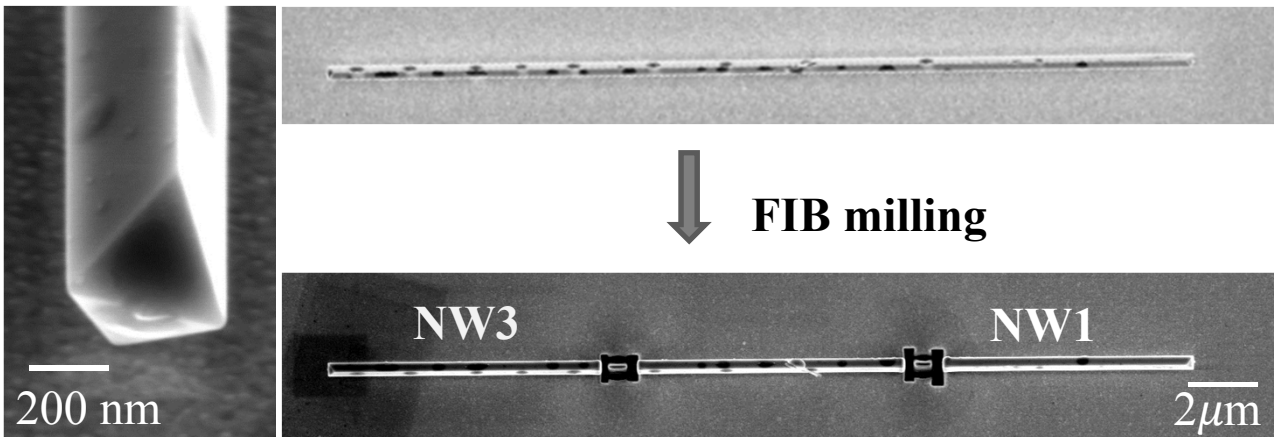

Figure S1. NW1 and NW3 are segments of the same MnSi NW (top right). This NW was cut with a focused ion beam (FIB) (bottom right) and then, under an optical microscope with precision micromanipulators, each segment was attached to a cantilever tip. The front view of the same wire (left).

	Nanowires		
	NW1	NW2	NW3
Configuration with respect to the field	Parallel	Parallel	Perpendicular
MnSi Nanowires			
Length [μm]	7.1	26.7	7.8
Volume [μm^3]	1.06	4.11	1.16
Demagnetization field [T]	0.0049 $\pm$ 0.0002	0.0014 $\pm$ 0.0001	0.0976 $\pm$ 0.0117
Si Cantilever			
Length l [μm]	180.0	180.0	180.0
Effective Length l_e [μm]	125.9	125.9	125.9
Resonant Frequency f_0 [Hz]	2062.8	2025.9	2106.3
Spring Constant k_0 [μN/m]	37 $\pm$ 5	50 $\pm$ 10	44 $\pm$ 10
Q-Factor Q_0 at T =4 K	4.1x10^4	4.0x10^4	4.2x10^4

Table S1. Properties of the MnSi wires and Si cantilevers for each measured configuration.

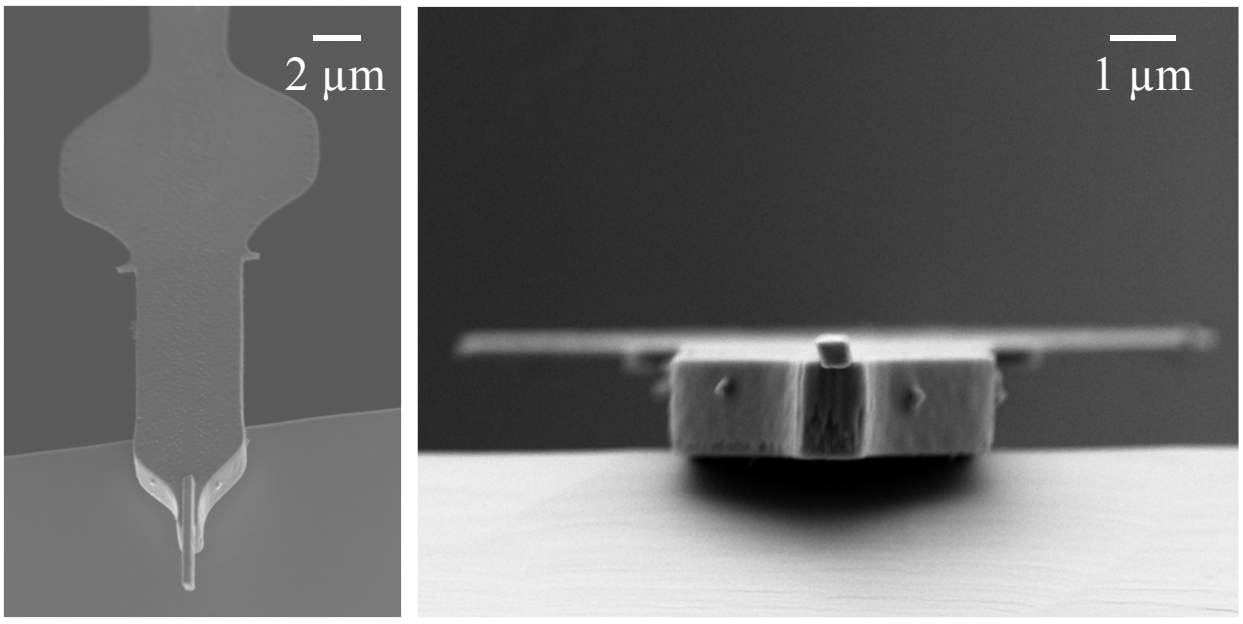

Figure S2. Scanning electron micrographs of NW1 attached to the tip of the cantilever, from the top (left) and the front (right).

IV. DETERMINATION OF PHASE TRANSITIONS

In order to determine the magnetic phase transitions from our measurements of MnSi NWs parallel to the applied magnetic field, $\Delta f(\mathrm{H})$ is first converted into $M(\mathrm{H})$. We next take note of the region in H and T showing sharp discontinuous dips in $M(\mathrm{H})$. We hypothesize that this behavior may be the signature of a mixture of skyrmion and conical or helical states. We therefore label this region in the phase diagrams shown in Figure S6 as the skyrmion mixed phase. Then we follow procedures similar to those described by Bauer and Pfleiderer for the determination of the transitions to the skyrmion lattice phase and to the FM phase[1]. We first remove the sharp dips associated with the mixed phase and fit the remaining $M(\mathrm{H})$ curve to a piecewise cubic spline. From this fit we calculate $\partial M/\partial H$. The removal of the sharp dips and the spline fit yield a $\partial M/\partial H$ which reveals the overall behavior of the magnetization. Next, moving from high field to low field, we identify the transition from FM to conical phase as the first point of inflection in $\partial M/\partial H$, e.g. around $H = 0.57$ T in Figure S3. Below this transition, the width of the dip in $\partial M/\partial H$ delineates the size of the skyrmion lattice phase. To quantify this width, we take the full-width at half-maximum (FWHM) as shown by the dotted lines in Figure S3.

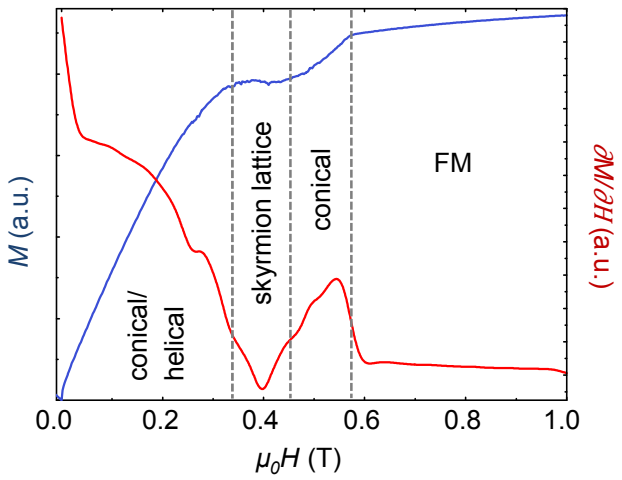

Figure S3. An example of $M(\mathrm{H})$ (blue) and the corresponding $\partial M/\partial H$ (red) used for determining magnetic phase transitions, here shown for NW1 at $T = 0.6$K (red).

In order to assign a transition between the conical and helical phases, we compare the ZFC and the FC data. Specifically, we compare Δf(H) and assign the transition to the field where the slope $(\partial \Delta f / \partial H)$ of the ZFC is equal to the slope of the FC, as shown in Figure S4.

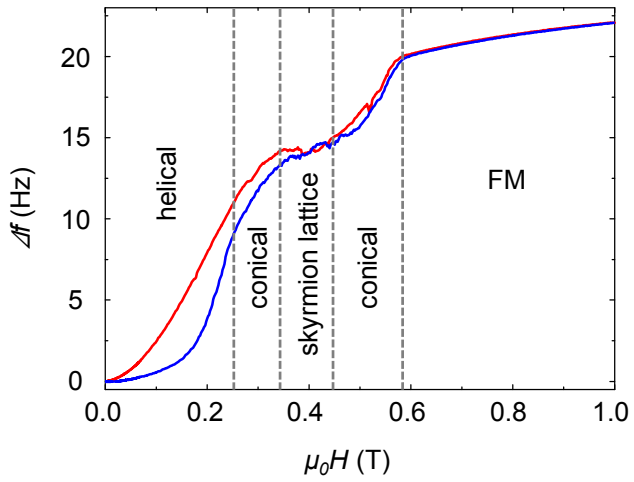

Figure S4. The frequency shift as a function of the applied magnetic field for a zero-field-cooled (ZFC) (blue) and a field-cooled (FC) (red) measurement of NW1 (long axis parallel to the field) at $T = 1.5$ K.

For measurements of MnSi NWs perpendicular to the applied magnetic field it is not possible to convert Δf (H) into M(H). Therefore in order to determine the extent of the various phases we start by taking note of the region in H and T showing sharp discontinuous dips in Δf (H) and label this region shown in Figure S7 the skyrmion mixed phase. Next, moving from high field to low field, we identify the transition from FM to conical phase as the discontinuous change in the slope of Δf(H), e.g. around $H = 0.42$ T in Figure S5. Below this transition, we identify the skyrmion lattice phase as a plateau bounded by the sharp discontinuities in Δf (H), which are characteristic of a first order phase transition. Once again, in order to assign a transition between the conical and helical phases, we compare the ZFC and the FC data. Specifically, we compare Δf and assign the transition to the field where the slope $(\partial \Delta f / \partial H)$ of the ZFC is equal to the slope of the FC, as shown in Figure S5.

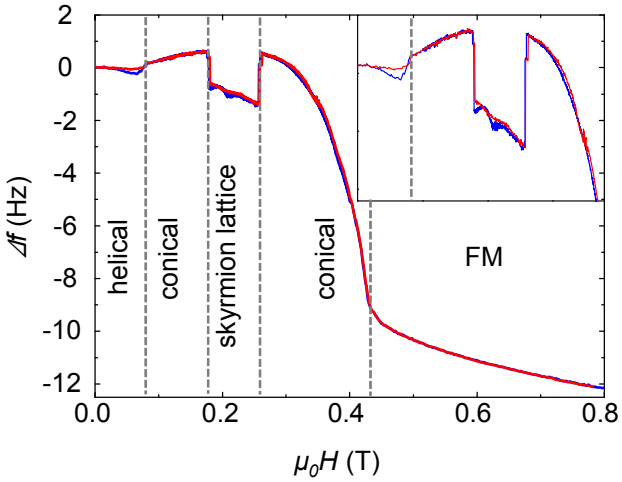

Figure S5. Δf (H) of NW3 (long axis perpendicular to the field) at $T = 27.5$ K. The skyrmion lattice phase is bounded by clear discontinuities in Δf (H) as expected for a first order phase transition. By comparing the zero-field-cooled (ZFC) (blue) and the field-cooled (FC) (red) data we assign the transition between the helical and the conical phase as described for the measurement of NW1, Figure S4.

V. PHASE DIAGRAMS WITH HELICAL-TO-CONICAL TRANSITION

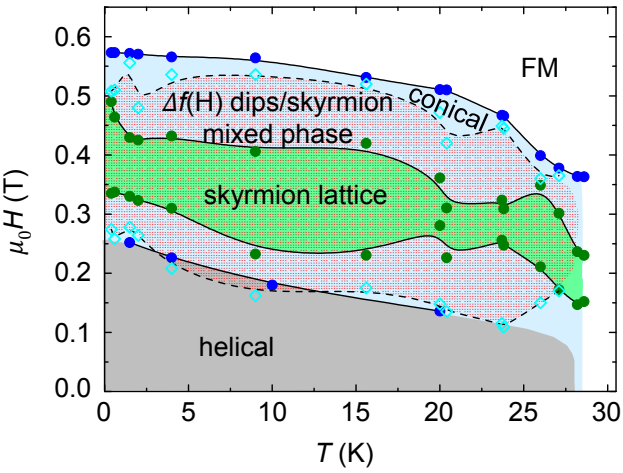

Figure S6. Extended skyrmion lattice phase for a MnSi NW parallel to the field (NW1). This phase diagram is identical to that shown in Figure 4 in the main text, with the addition of the boundary between the helical and conical phase. This boundary is determined through comparison of FC and ZFC measurements as discussed in section IV.

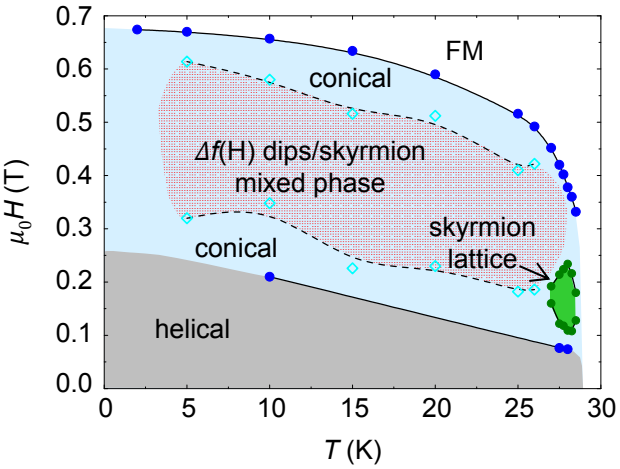

Figure S7. Skyrmion lattice phase for a MnSi NW perpendicular to the field (NW3). This phase diagam is identical to that shown in Figure 6 in the main text, with the addition of the boundary between the helical and conical phase. This boundary is determined through comparison of the FC and ZPC measurements as discussed in section IV.

REFERENCES

[1]A. Bauer and C. Pfleiderer, *Phys. Rev. B* **85**, 214418 (2012).